JSAT
Journal of Science and Agricultural Technology
Research Article
https://doi.org/10.14456/jsat.2023.8
e-ISSN 2730-1532, ISSN 2730-1524

Adsorption of methylene blue dye onto the natural liquid sugars-based carbon: Kinetic and thermodynamic

Atit Wannawek[1*], Yanee Keereeta[1], Pongthep Jansanthea[2], Watee Panthuwat[1], Tanongsak Sassa-deepaeng[1,3], and Pusit Pookmanee[4,5]

[1]Faculty of Science and Agricultural Technology, Rajamangala University of Technology Lanna, Lampang 52000, Thailand
[2]Program in Chemistry, Faculty of Science and Technology, Uttaradit Rajabhat University, Uttaradit 53000, Thailand
[3]Agricultural Biochemistry Research Unit, Faculty of Science and Agricultural Technology, Rajamangala University of Technology Lanna, Lampang 52000, Thailand
[4]Department of Chemistry, Faculty of Science, Maejo University, Chiang Mai 50290, Thailand
[5]Nanoscience and Nanotechnology Research Laboratory (NNRL), Faculty of Science, Maejo University, Chiang Mai 50290, Thailand

***Corresponding author**: atit_wannawek@rmutl.ac.th*

Received: March 27, 2023. Revised: May 29, 2023; July 12, 2023. Accepted: October 20, 2023.

ABSTRACT

In this research, glucose-based carbon, fructose-based carbon, and sugarcane juice-based carbon materials were successfully synthesized by a simple, rapid, and one-step reaction for methylene blue adsorption. The samples were produced by the reaction of sugarcane juice with sulfuric acid. The characterization of the synthesized samples was performed by scanning electron microscopy (SEM), energy dispersive spectroscopy (EDS), Fourier Transform Infrared Spectroscopy (FTIR), and nitrogen adsorption-desorption analysis (BET). The adsorption behaviors of all samples were investigated by the determination of the adsorption capacity of methylene blue. The optimum condition for the highest adsorption capacity was at pH 7 and a contact time of 480 min. The kinetic and adsorption isotherms and thermodynamics of methylene blue on all samples were studied. Pseudo-second-order and Langmuir's isotherm were best fitted for methylene blue removal. This is indicated by chemical and monolayer adsorption. The mechanism of the adsorption process can be illustrated by the intra-particle diffusion model. A study of the thermodynamic parameters showed positive enthalpy (ΔH) and entropy (ΔS) values. This suggested that endothermic adsorption processes increased the randomness of adsorbate and adsorbent. Additionally, the negative value of Gibbs free energy (ΔG) indicated a spontaneity of adsorption. The presence of salts (NaCl and $MgCl_2$) and coexisting ions (Pb^{2+} and Zn^{2+}) cause a decrease in the adsorption efficiency.

Keywords: adsorption, carbon, sugarcane juice, sulfuric acid, methylene blue

INTRODUCTION

Wastewater discharge from chemical industries has been a continuous, long-standing problem. Mainly, dye product usage in several industries has inevitably caused environmental pollution. The dyes block the sunlight from entering the water and interrupt the ecosystem. On the other hand, some dyes are invisible and later become toxic and carcinogenic over prolonged exposure (Tuli et al., 2020). Dyes commonly used in the textile industry, such as methylene blue, congo red, remazol black, and remazol red, harm ecosystems and organisms, mainly aquatic life. This may eventually affect public health (Amran and Zaini, 2021). Methylene blue (3,7-bis(dimethylamino)-phenothiazin-5-ium chloride) (Noreen et al., 2020), thiazine cationic dye, is significant for colors manufacturing applied for paper, cotton wool, and wool. The amino group with positively charged methylene blue is toxic to plants and animals (Aramesh et al., 2021). Therefore, the treatment of water contaminated with dyes has been focused. Currently, there are many treatment technologies for dye removal from wastewater, such as aerobic treatment systems, chemical oxidation, ozonation, sedimentation, ultrafiltration, membrane filtration, flocculation, ion exchange, biodegradation, electrochemical degradation, photocatalytic degradation, and adsorption. Some methods are, however, expensive, time-consuming, and technically complicated (Wu et al., 2021).

Adsorption technology has been proficiently developed. This method has been extensively used in wastewater treatment due to its environmentally friendly operation, high efficiency, and worthiness (Adekola et al.,2019). Various adsorbents have been studied to remove pollutants from wastewater including nanoparticles (Arab et al., 2022), nanocomposites (Khushboo et al., 2022), polymer

materials (Sattari et al.,2021), magnetic composites (Kumar et al., 2021), graphene oxide (Gautam and Hooda, 2020), graphite (Corona et al., 2021), activated carbon (Sultana et al., 2022), etc. Carbon and activated carbon (AC) are significant materials with adsorption properties due to their porosity, high surface area, and surface chemical characteristics. Therefore, there is interest in developing new carbon-based materials produced directly from plant-based materials, such as palm oil wood, palm kernel fiber, cashew nut, corncob, hazelnut husk, and others (Bello et al., 2021). The properties of these activated carbons depend on the type of raw material, operating time of the carbon process, temperature, and activating agent (Bergna et al., 2020).

NaOH, KOH (base activation), and H_2SO_4 (acid activation) are the most commonly used activating agents. In addition, the latter is a great alternative activating agent because of its efficiency of excellent methylene blue adsorption (Nizam et al., 2021). Activated carbon is produced by the chemical activation of sucrose, which is high-performance for adsorption (Bedin et al., 2016). Recently, various methods have been studied in synthesizing hydrochar and activated carbon for the adsorption of iodine and methylene blue (Genli et al., 2021).

The problem of smoke haze pollution is biomass burning (Khodmanee and Amnuaylojaroen, 2021) and charcoal/biochar production (Sparrevik et al., 2015). Using sulfuric acid during dehydration to prepare adsorption carbon is an alternative option to avoid problems caused by burning. It is well-known that carbohydrate dehydration is a simple and fast reaction (Dolson et al., 1995). For this reason, the reaction of sugar with sulfuric acid is a famous chemistry experiment. The sugar dehydration reaction for carbon film production was presented as a straightforward and rapid method (Whitener, 2016).

Natural products are relatively safe and eco-friendly products. The adsorbent carbons from solid natural products have been widely studied (Suhas et al., 2016). Natural liquid sugars-based carbon is another interesting option. Inverted sugar is present in natural liquid sugar derived from fruit (Naikwadi et al., 2010), which reacts rapidly with H_2SO_4 and reduces smoke haze pollution, especially when sugarcane juice is available throughout the country. It contains inverted sugar hydrolyzed to glucose and fructose by acidifying and can be rapidly carbonized by a dehydration reaction with H_2SO_4. Sugarcane juice has a high sugar content and can spoil quickly after extraction (Zaidan et al., 2021). Freshly squeezed sugarcane juice is easily spoiled and has a shelf life of only a few hours (Geremias-Andrade et al., 2020). For this reason, using a nearly expired sugarcane juice is a value-added.

In this study, sugarcane juice is represented as a natural product due to its high inverted sugar content. The glucose powder-based carbons (GBC), saturated glucose solution-based carbons (GSBC), fructose powder-based carbons (FBC), saturated fructose solution-based carbons (FSBC), and sugarcane juice-based carbons (SJBC) were synthesized by a chemical reaction using concentrated H_2SO_4. All samples were characterized by SEM, EDS, FTIR, and BET analysis. The adsorption behaviors of the samples were investigated by adsorption of methylene blue dye and compared with GBC, GSBC, FBC, FSBC, and SJBC. In addition, the kinetics, adsorption isotherms, thermodynamics, effect of salts, and coexisting ions were studied.

MATERIALS AND METHODS

Materials

The sugarcane juice derived from the crushed sugarcane (*Saccharum officinarum*, Suphanburi 50) by sugarcane hydraulic press. This sugarcane was harvested from Ban Thung Ku Dai, Pong Saen Thong, Muang Lampang, Lampang Province, Thailand (18.296914,99.432422). Glucose powder ($C_6H_6O_{12}$, 99.0%, Ajax Finechem Pty Ltd., Australia), fructose powder ($C_6H_6O_{12}$, 99.0%, Ajax Finechem Pty Ltd., Australia), and sulfuric acid (H_2SO_4, 98.0% ACL Chem Ltd., England) were used as precursors in the experiments. The pH-adjusted reagents were prepared with sodium hydroxide (NaOH, 99.0%, RCI Labscan., Thailand) and nitric acid (HNO_3, 70% Ajax Finechem Pty Ltd., Australia). Hydrochloric acid (HCl, 37.0% RCI Labscan Ltd., Thailand), potassium sodium tartarate-4-hydrate (Merck, Darmstadt), 3,5-dinitrosalicylic acid (DNS, 98% Sigma Aldrich Co., USA), and potassium hydroxide pellets (KOH, 85% Loba Chemie Ltd., India) were used for sugarcane juice hydrolyzation and sugar analysis. Sodium nitrate ($NaNO_3$, 99.5% RFCL Ltd., India) was employed to determine pH_{zpc} values. Sodium chloride (NaCl, 99% RCI Labscan Ltd., Thailand) and magnesium chloride ($MgCl_2$, 98% RCI Labscan Ltd., Thailand) were used for the study of the effect of salts on methylene blue adsorption. For the impact of coexisting ions on methylene blue adsorption, lead chloride ($PbCl_2$, 99% RCI Labscan Ltd., Thailand) and zinc chloride ($ZnCl_2$, 98% QRëC, New Zealand) were used for this study. In preparing the adsorption and kinetics study solution, methylene blue trihydrate

($C_{16}H_{18}N_3S.Cl.3H_2O$, 99.0%, Himedia Laboratories Pvt Ltd., India) was used as adsorbate. All solutions in this experiment used deionized water (DI) as the solvent.

Preparation of adsorbents

The carbon material was prepared without heating (Whitener, 2016). GBC GSBC FBC and FSBC were prepared by slowly adding 50 mL of concentrated sulfuric acid to each of the large beakers, which contained 50 g of glucose powder, saturated glucose solution (50 g of glucose), 50 g of fructose powder and saturated fructose solution (50 g of fructose), respectively. The individual carbon samples were separated, washed with deionized water, and dried in a hot-air oven at 95 °C for 24 h. Similarly, SJBC was prepared by adding concentrated sulfuric acid to sugarcane juice (12% of reducing sugar) in a 2 L beaker. The carbon from this process was separated by filter paper. It was washed and dried at 95 °C for 24 h in a hot air oven. All of the carbon samples were stored in a desiccator.

Characterization

All samples are powdered and characteristically examined by SEM, EDS, FTIR, and BET techniques. The morphology was investigated using a scanning electron microscope (TESCAN–VEGA3, Czech Republic) at 5.0 kV. The chemical composition of the samples was obtained by using an energy dispersive spectroscopy (Oxford Instrument-Ultim Max 40, England) and Fourier-transform infrared spectroscopy (PerkinElmer/Spectrum RX I, UK), which were performed in wavenumber between 400 and 4000 cm^{-1} with KBr pellets. The surface areas were calculated with the BET method. The adsorption-desorption analysis of nitrogen was carried out by using a surface area, pore volume, and pore size analyzer (Quantachrome-Autosorp 1MP, England) at an adsorber temperature of −196 ºC, out gas temperature: 120 ºC, outgas time 8 to 24 h and operating time 382.1 to 389.4 min. Sugarcane juice (SJ) was hydrolyzed and then analyzed for sugar content by DNS method (Wang, 2004; Texixeira and Santos, 2022). Briefly, the 1,000 µL of SJ was firstly chemically digested by adding 20 µL of concentrated HCl and then placed in a 90 ºC hot water bath for 5 min. After cooling it to ambient temperature, 50 µL of 5 N KOH solution was added to neutralize the acid. The colorimetric reaction was carried out in the 5 mL test tubes using 0.5 mL of sample or reference solution (between 0.1 and 0.3 gL^{-1} of glucose) and 0.5 mL of DNS reagent. After mixing by vortex, all samples were boiled in a 95 ºC hot water bath for 5 min and cooled to ambient temperature. The absorbance was measured at 540 nm using a V-1200 spectrophotometer (Dshing Instrument Co., Ltd., China) with UV-Professional analysis software. All experiments were carried out in triplicates. Determination of zero-point charge (PZC) was applied to evaluate the effect of pH on the adsorption between the surface charge of adsorbent and adsorbate. The solutions of 0.1 mol/L $NaNO_3$ solutions 40 mL were adjusted in the initial pH values (pH_i) range of 2, 4, 6, 8, 10, and 12 using 0.1 M NaOH and 0.1M HNO_3. 0.1 g of adsorbent was added to all solutions. The suspensions were shaken at 120 rpm for 24 h. The final solutions were separated and recorded final pH values (pH_f). The pH_{zpc} was obtained by plotting between pH_i and ΔpH.

Adsorption studies

Effect of pH

The influence of pH was investigated by adding 0.05 g of adsorbent to the 40 mg/L of methylene blue solutions (25 mL) over the pH range from pH 2 to 9, which were adjusted by pH 0.1 M NaOH and 0.1 M HNO_3. The samples were shaken at 120 rpm for 24 h.

Effect of contact time

The effect of the contact time experiment was performed by varying contact times from 5 to 1440 min at optimum pH from effect of the pH study. Each Erlenmeyer flask contained 25 mL of fixed methylene blue concentration (40 mg/L) and 0.05 g of adsorbent. The samples were shaken at 120 rpm.

Effect of initial concentration

The Effect of the initial concentration study was operated under optimum conditions (pH of 7 and contact time 480 min) and varying initial concentrations of methylene blue from 5 to 80 mg/L. Adsorbent (0.05 g) was added to each Erlenmeyer flask containing 25 mL of methylene blue. The samples were shaken at 120 rpm.

Thermodynamic study

The effect of temperature was studied using a temperature range of 25 to 55 °C, pH of 7, and contact time of 480 min. The 0.05 g of adsorbent was added to the 40 mg/L of methylene blue solutions 25 mL. The samples were shaken at 120 rpm.

Effect of salts and coexisting ions

The effect of salt and coexisting ions was studied under optimum conditions. The impact of the salt study, the difference of NaCl (5 to 10 g/L) and $MgCl_2$ was added to the Erlenmeyer flask, which contained methylene blue solution (25 mL, 40 mg/L)

and 0.05 g of adsorbent. The effect of coexisting ions was performed by varying concentrations of Pb^{2+} and Zn^{2+} from 10 to 40 mg/L, which were prepared from 200 mg/L stock solutions of Pb^{2+} and Zn^{2+}, respectively. The samples were shaken at 120 rpm and a contact time of 480 min.

The final samples were centrifuged at 6,000 rpm to separate the solutions and solids. The absorbance values of the final solutions were measured by UV/Vis spectrometer (Metash V-5800, China) at wavelength 664 (Oladoye et al., 2022). The data of absorbance were used to calculate the final concentration and applied to kinetic and adsorption isotherm studies.

RESULTS AND DISCUSSION

Characterizations of the prepared adsorbents

Results of SEM and EDS

The morphology of carbons can be evaluated using SEM–analysis. The SEM photographs of all samples are shown in Figure 1. The morphology of GBC and FBC surfaces was compact, dense, layer-like, and rough, as shown in Figures 1(a) and 1(c). The characteristics of this morphology are similar to those of carbons, which were produced using an acid mixture of H_2SO_4 and H_2O_2 and analyzed by SEM technique (Chalmpes et al., 2022). The morphology of GSBC and FSBC surfaces was an agglomeration of small granules, as seen in Figures 1(b) and 1(d). This indicates that GSBC and FSBC have high surface area and are more porous than GBC and FBC, which is consistent with BET results. The surface texture (Figure 1(e)) was formed by aggregating tiny particles more compact than those of GSBC and FSBC. It is observed that SJBC has less pore size than GSBC and FSBC, as the surface area and the pore number influence adsorption. The elemental composition of all carbon samples was investigated by EDS spectroscopy, as shown in Figure 1, which consists of carbon and oxygen as the main constituents. To the EDS results, the similar O/C ratios of GBC, GSBC, FBC, FSBC, and SJBC were 0.345, 0.349, 0.378, 0.374, and 0.373, respectively. This indicates the oxygen content in the functional group. The oxygen on the charcoal surface resulted in a negatively charged surface. This caused the attraction between the adsorbent and methylene blue through an electrostatic mechanism so that the elimination was promoted (El-Bery et al., 2022). Sulfur(S) and gold(Au) peaks remain their precursors and gold sputter coating technique of SEM, respectively.

Results of FTIR

The functional groups present in all samples were investigated by the FTIR, as shown in Figure 2. The absorbance bands peaked around 3401 $cm^{-1,}$ corresponding to the strong O–H stretching of alcohol (Mondal and Majumder, 2019). The band located at about 2921, 1704, 1581, and 1160 cm^{-1} were assigned C–H stretching of alkane, carbonyl C=O groups of carboxylate asymmetric/symmetric stretching, C=C stretching and C–O stretching, respectively (El Maataoui et al., 2019; Marrakchi et al., 2020; Opoku et al., 2021). The absorbance peak around 1200 to 800 and 956 cm^{-1} was described as the C–C stretching and the trans-out-of-plane bending of C=C–H (Wibawa et al., 2020). The peak of about 789 and 580 cm^{-1} may be caused by carbonaceous agglomeration (Samoudi et al., 2022). The FTIR results indicated that all the samples contained carbon and oxygen, which was consistent with the results from the EDS. The peak positions of all samples are similar. It seems promising to have identical functional groups, including carboxylate and hydroxyl groups. A peak at 956 cm^{-1} was not found in GBC and GSBC. The peak was, however, observed in SJBC. This is probably because it was produced from sugarcane juice, which contains glucose and fructose.

The methylene blue dye cation (MB^+) adsorption onto all carbon samples occurred, representing the carboxyl, carboxylate, and hydroxyl groups (Wang et al., 2018). The carboxylic and hydroxyl groups become hydroxyl anion and carboxylate anion in an aqueous solution (Namal and Kalipci, 2020). These groups can actively interact with cations such as methylene blue (Dhar et al., 2021).

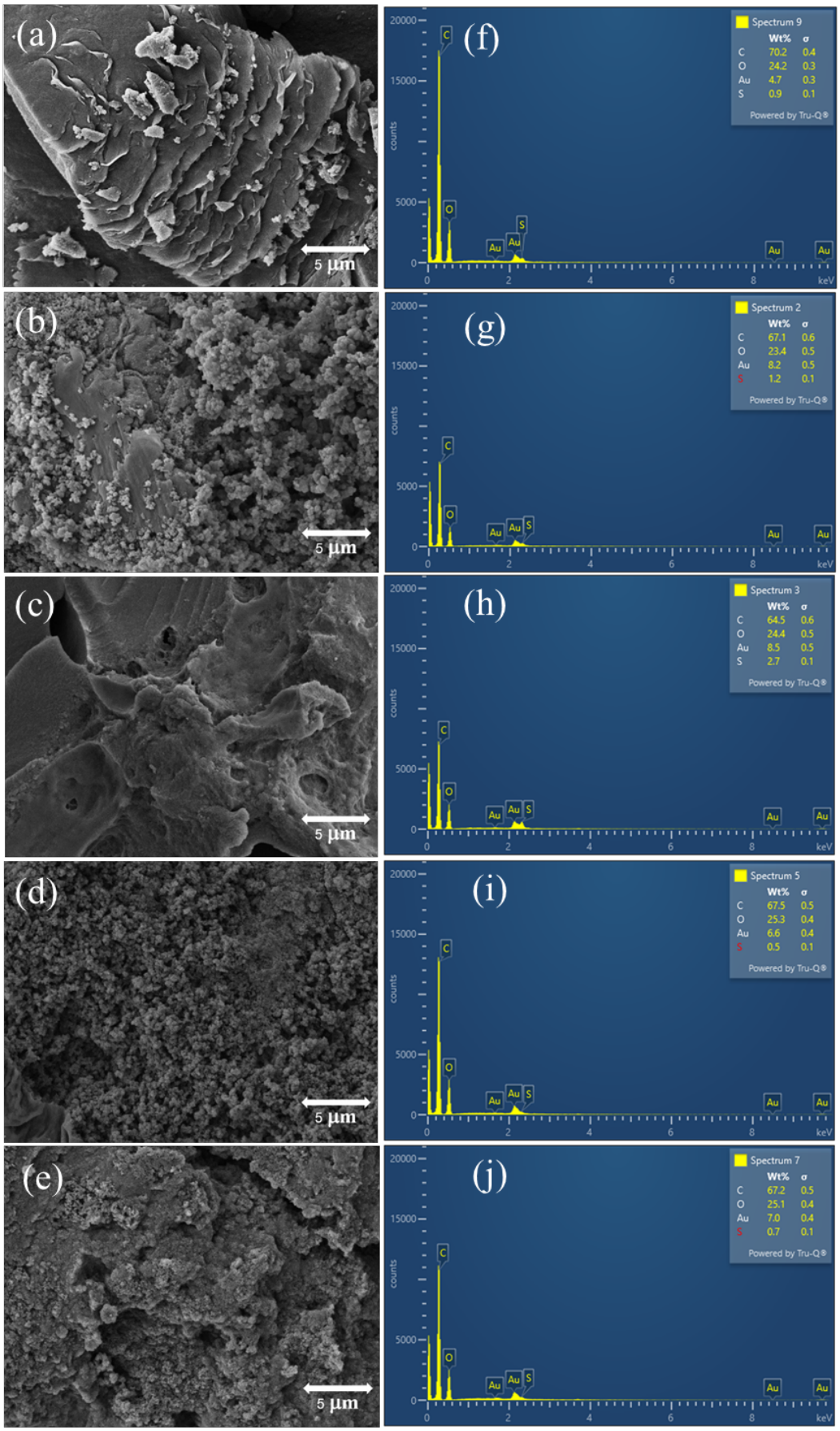

Figure 1. SEM photographs of GBC (a), GSBC (b), FBC (c), FSBC (d), and SJBC (e) and EDS results of GBC (f), GSBC (g), FBC (h), FSBC (i) and SJBC (j).

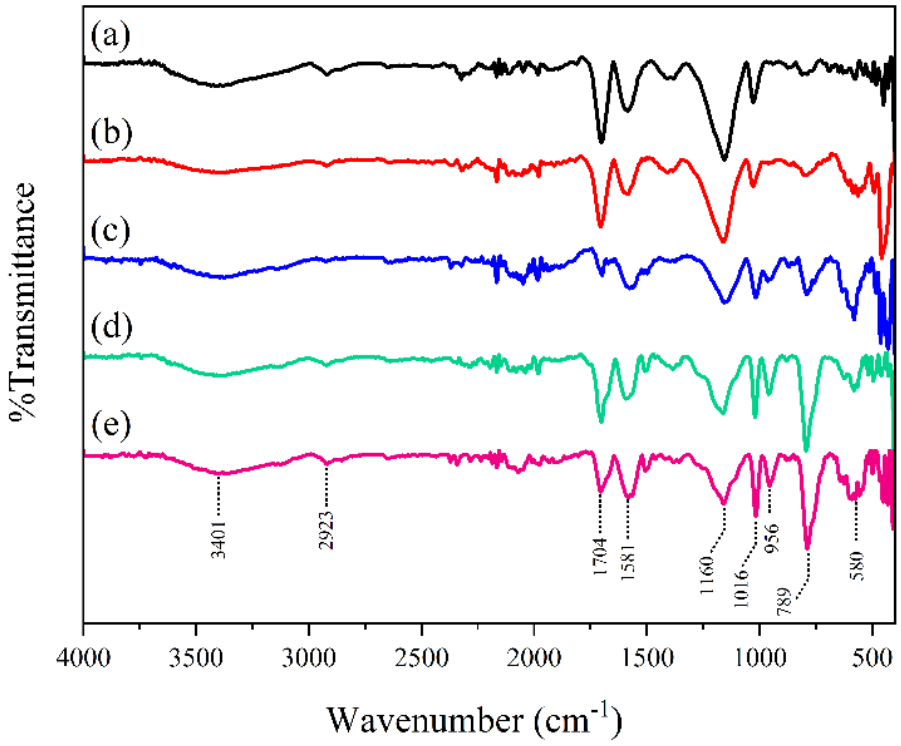

Figure 2. FTIR spectra (KBr disc) of GBC (a), GSBC(b), FBC(c), FSBC(d) and SJBC(e).

Results of nitrogen adsorption-desorption

The specific surface area (S), pore volume (Vp), and average porous radius of GBC, GSBC, FBC, FSBC, and SJBC are summarized in Table 1. After the solution process of glucose and fructose powder and hydrolysis with conc. H_2SO_4, the specific surface area and pore volume of GSBC and FSBC were further increased compared to GBC and FBC, respectively. The specific surface area and pore volume can indicate the physical adsorption capacity of materials. The specific surface area result corresponded with SEM results, which showed aggregation of small particles for GSBC, FSBC, and SJBC. The specific surface area of all samples is greater than that of the carbon produced by the chemical reaction (spent coffee and piranha solution), which was reported previously (10–15 m^2/g) (Chalmpes et al., 2022). The specific surface area depends on porosity, pore size distribution, shape, size, and roughness (Amador et al., 2016). The specific surface area of the particles affects the adsorption efficiency; the high specific surface area causes increased adsorption (Thang et al., 2021). However, the pore-volume and average radius of the porous also affect adsorption.

Table 1. BET constants for GBC, GSBC, FBC, FSBC, and SJBC

Adsorbent	S (m^2/g)	V_p (cm^3/g)	Average radius of porous (Å)
GBC	24.82	0.0454	36.56
GSBC	35.98	0.0947	52.66
FBC	23.52	0.0415	35.27
FSBC	24.92	0.0783	62.87
SJBC	20.92	0.0504	48.20

Effect of pH on the adsorption of methylene blue

The effect of pH was studied within a pH range of 2 to 9 at the methylene blue concentration of 40 mg/L, 25 ºC, and contact time of 24 h. As shown in Figure 3(a), The methylene blue adsorption of all samples tended to be the same pattern. Conversely, the adsorption capacity seems to increase with an increase in pH and stabilize at pH > 7. The pH_{pzc} values of GBC, GSBC, FBC, FSBC, and

SJCB were determined from a final pH (pH_f) as a function of initial pH (pH_i). The pH_{pzc} value revealed the characteristic of charges on the adsorbent surface. It is indicated that when pH of the solution (pH) is higher than pH_{pzc}, the surface provides a negative charge. On the other hand, the surface shows a positive charge when pH of the solution is lower than pH_{pzc} (Zhang et al., 2021). Figure 3 suggested the point of zero charges of GBC, GSBC, FBC, FSBC, and SJCB, which were 5.4, 5.5, 5.8, 5.5, and 5.5, respectively. The adsorbent surface at pH > pH_{pzc} with a negative charge was affected by electrostatic pulling between the adsorbent surface and methylene blue. Electrostatic interactions have been described on the principle of a charge density on the adsorbent surface, which is correlated with zeta potential. The deprotonation of hydroxyl and carboxyl groups will increase the negative charge density on the adsorbent. This facilitates electrostatic interaction between the adsorbent and cation of methylene blue (Gautam and Hooda, 2020).

At low pH, the solution was obtained with high concentrations of H_3O^+. The decreasing adsorption capacity was detected due to the competition of positive ion effect between H_3O^+ and methylene blue (Zhou et al., 2018). The electrostatic repulsion between methylene blue, a cationic dye, and the adsorbent surface increased due to the increase in the H_3O^+ concentration (Alver et al., 2020). However, when pH < pH_{pzc} is considered, the surface of the adsorbent becomes positively charged. This induces an electrostatic repulsion on the free H_3O^+ ions in the solution and the cation of methylene blue (Gautam and Hooda, 2020).

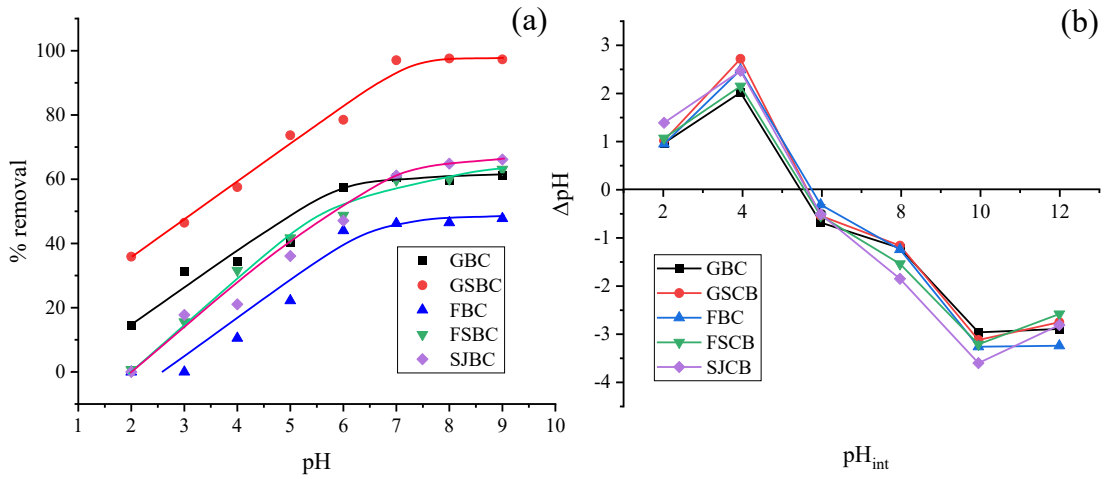

Figure 3. Effect of pH (a), pHpzc determination curve of GBC, GSBC, FBC, FSBC and SJBC (b).

Effect of contact time and initial concentration of adsorbents

The effect of contact time at different contact times of 5, 10, 20, 30, 40, 50, 60, 120, 240, 360, 480, and 1440 min was investigated at the methylene blue concentration of 40 mg/L, pH of 7 and 25 ºC. The percent removal of methylene blue is shown in Figure 4(a). It was found that the trend of methylene blue adsorption to all adsorbents was in the same pattern. The methylene blue was adsorbed rapidly in 0 to 50 min due to the fact that all samples consisted of abundant free adsorption sites and the electrostatic interaction effect between molecules of the adsorbates and adsorption sites on the adsorbent (Lyu et al., 2020). After a while, the adsorption sites were filled with methylene blue. The gradual increase of the methylene blue adsorption was shown for 50 to 240 min due to the decrease of adsorption sites and the repulsion of methylene blue in solution and methylene blue absorbed on the adsorption sites (Nkutha et al., 2020). A slower adsorption rate was observed for 240–360 min afterward because the adsorption sites were nearly filled with methylene blue molecules. After 360 min, the adsorption of methylene blue was continuing. However, the process was occurred at a lower rate and prolonged before entering an equilibrium. Therefore, this study assumed that at 480 min, the adsorption occurred close to an equilibrium point to reduce the study time length for other adsorption-affected factors. However, the adsorption had entered equilibrium, and the treatment would later no longer be able to eradicate methylene blue.

A study of initial concentrations was conducted under varying concentrations of methylene blue. The different initial concentrations of 5, 10, 20, 30, 40, 50, 60, 70, and 80 mg/L of all samples were examined at 25 ºC, pH of 7, with a contact time of 480 min. Figure 4(b) shows that the amount of removed methylene blue varies with different initial concentrations. The adsorption capacity of methylene blue on all samples was the same pattern. It increased as the initial concentration increased, and it eventually became stable. The higher initial concentration resulted in a higher amount of removed methylene blue was observed. This is due to the driving force generated by increasing solute, which is sufficient to overcome the mass transfer resistance between the solid and liquid phases. This will remain stable after reaching equilibrium. However, the adsorption capacity decreased at the initial 70 mg/L concentration. This may be due to a repulsion between methylene blue on the adsorbent surface and methylene blue in a solution.

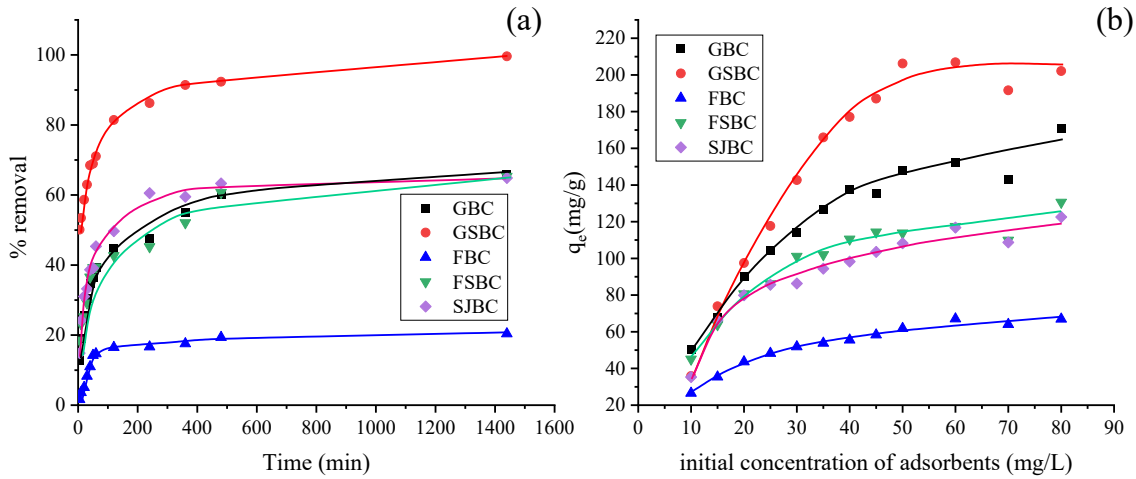

Figure 4. Effect of contact time (a) and initial concentration of methylene blue removal (b).

Kinetic study

The contact time data of methylene blue adsorption onto all adsorbents were used to study adsorption kinetic. The pseudo-first-order, pseudo-second-order, and intra-particle diffusion models were evaluated by equations (1), (2), and (3), respectively (Badri et al., 2020; Tran et al., 2020).

$$\log(q_e - q_t) = \log(q_e) - \frac{k_1}{2.303}t \quad (1)$$

$$\frac{t}{q_t} = \frac{1}{k_2 q_e^2} + (\frac{1}{q_e})t \quad (2)$$

$$q_t = k_{ip}t^{1/2} + C \quad (3)$$

Where t, q_e, and q_t are contact time, adsorption capacity (mg/g) at equilibrium, and at a time "t," respectively. The k_1, k_2, and k_{ip} represent the rate constant of pseudo-first-order, pseudo-second-order, and intra-particular-diffusion models. The C is maintaining the boundary layer thickness. The data were plotted for the three models, shown in Figure 5, and the obtained kinetic parameters were summarized in Table 2. The methylene blue adsorption on all adsorbents follows the pseudo-second-order model, which was fitted due to the calculated value (q_{cal}) high approximation with the experimental data (q_{exp}) and better linearity (high R^2) than the pseudo-first-order model. Therefore, the pseudo-second-order model was suitable to explain better the adsorption kinetics of methylene blue adsorption by GBC, GSBC, FBC, FSBC, and SJBC. The pseudo-second-order model can be used for predicting adsorption capacity. The expected value is similar to those of the experiments. The pseudo-second-order model demonstrated a chemisorption process involving electrostatic force and valence forces (Sahoo and Prelot, 2020). For SJBC, the adsorption capacity values obtained from the experiment and the pseudo-second-order model were 135.1 and 133.4 mg/g. However, the intra-particle diffusion model showed the potential control rate and diffusion mechanism of the adsorption process. This indicated intra-particle diffusion during the adsorption process. The parameters are given in Table 3. The two steps of adsorption were illustrated as the intra-particle diffusion model. The slope of

the line for the first step occurred at 5 to 60 min ($t^{1/2}$, 2.24 to 7.75 $min^{1/2}$). This suggested that methylene blue is rapidly adsorbed on the surface of the adsorbent. The second step occurred approximately 120 min and 1440 min ($t^{1/2}$, 11.0 to 37.9 $min^{1/2}$). The particles were diffused within the adsorbent. The slope was increased gradually, as well as the adsorption, until equilibrium. This is a progressive and speed-limiting step of the intra-particle diffusion process. The experimental results were similar to those from the adsorption of methylene blue by Coal-based activated carbon reported by Wang et al. (2022), which showed a rapid adsorption rate in the first step and a decreasing rate in the second step model.

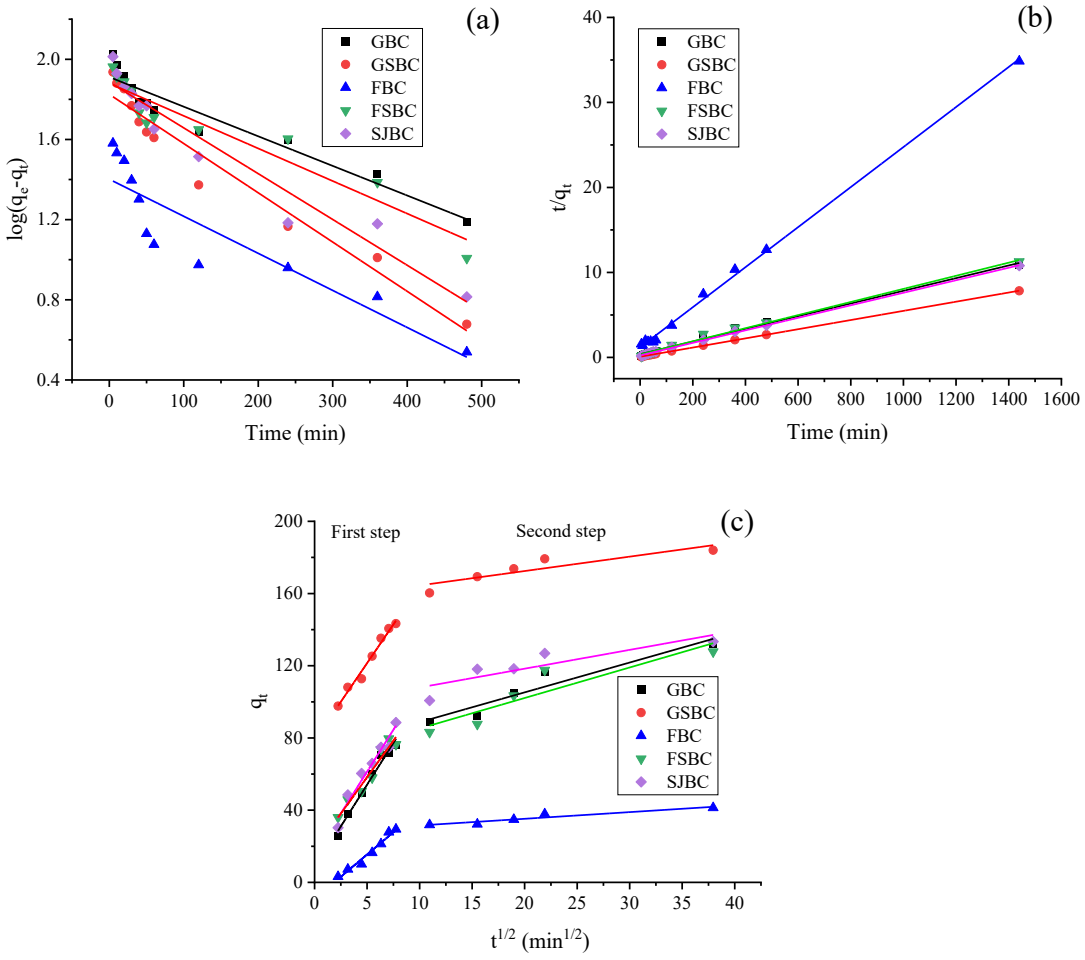

Figure 5. Kinetic plots of methylene blue removal for the pseudo-first-order (a), pseudo-second-order (b), and intra-particle diffusion (c).

Table 2. The obtained kinetic parameters for the adsorption of methylene blue onto GBC, GSBC, FBC, FSBC, and SJBC using pseudo-first and pseudo-second-order models

Adsorbents	Parameters							
	Pseudo-first-order				Pseudo-second-order			
	k_1 (L/min)	$q_{e(cal)}$ (mg/g)	$q_{e(exp)}$ (mg/g)	R^2	$k_2 \times 10^{-4}$ (g/mg min)	$q_{e(cal)}$ (mg/g)	$q_{e(exp)}$ (mg/g)	R^2
GBC	0.0035	81.51	132.0	0.9198	2.81	117.6	132.0	0.9907
GSBC	0.0058	66.87	184.0	0.9551	3.61	185.2	184.0	0.9998
FBC	0.0041	25.21	41.30	0.8119	4.67	42.4	41.3	0.9982
FSBC	0.0037	75.88	127.8	0.9086	1.68	129.9	127.8	0.9943
SJBC	0.0053	76.93	133.4	0.9432	2.31	135.1	133.4	0.9994

Table 3. Intra-peptide diffusion parameters for the adsorption of methylene blue onto GBC, GSBC, FBC, FSBC, and SJBC

Adsorbents	Parameters					
	First step			Second step		
	k_{ip} (mg/g min$^{1/2}$)	C	R^2	k_{ip} (mg/g min$^{1/2}$)	C	R^2
GBC	0.0035	81.51	0.9198	2.81	117.6	0.9907
GSBC	0.0058	66.87	0.9551	3.61	185.2	0.9998
FBC	0.0041	25.21	0.8119	4.67	42.4	0.9982
FSBC	0.0037	75.88	0.9086	1.68	129.9	0.9943
SJBC	0.0053	76.93	0.9432	2.31	135.1	0.9994

Adsorption isotherms study

The adsorption isotherms were studied at 25 ºC, pH of 7, and contact time of 480 min. The concentrations of methylene blue were 10, 15, 20, 25, 30, 35, 40, 50, 60, 70, and 80 mg/L, respectively. Figure 6(a) shows that the adsorption of methylene blue was a rapid process at the first step due to the presence of abundant active sites (carboxylate and hydroxyl groups) evident in the FTIR result. The adsorption capacity was constant when it reached the equilibrium state. Adsorption isotherms of solids were related to the amount of adsorption and the concentration of a solution. The Langmuir isotherm is relevant to homogeneous sites and monolayer adsorption, a definite position, and several adsorbed molecules, and the adsorbed molecules can adsorb only one molecule. The Freundlich isotherm can be used for heterogeneous surfaces, which is multilayer adsorption (Kalam et al., 2021). The Langmuir and Freundlich isotherms were interesting and shown in equations (4) and (5) (Rehman et al., 2021; Rheima et al., 2021).

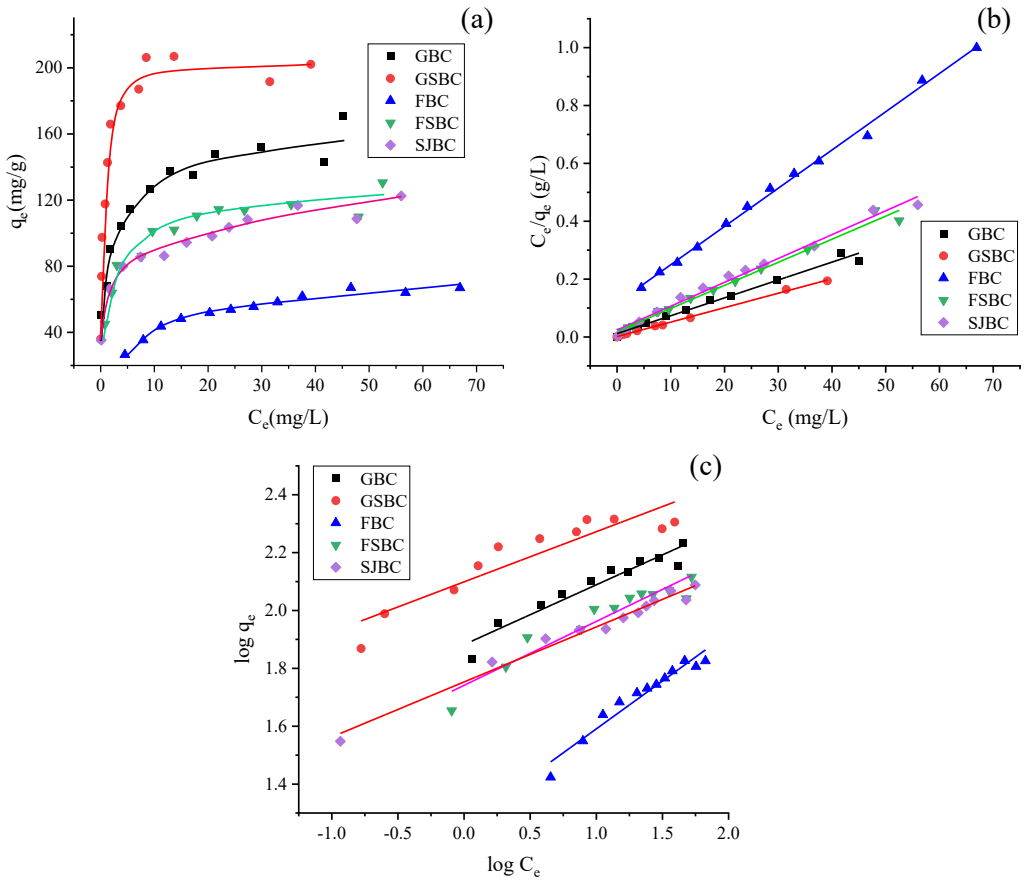

Figure 6. Adsorption isotherm of methylene blue removal (a), Langmuir (b), and Freundlich isotherm (c).

$$\frac{C_e}{q_e} = \frac{1}{q_m b} + \frac{C_e}{q_m} \quad (4)$$

$$\log q_e = \log K_F + \frac{1}{n}\log C_e \quad (5)$$

Where q_m is the maximum adsorption capacity (mg/g), C_e represents the methylene blue concentration at equilibrium, and b and K_F are the Langmuir and Freundlich constant, respectively. The Langmuir constant (b) refers to the adsorbate and surface interaction. The large value of b presents a strong interaction between the adsorbate and the adsorbent. The small b value presents a weak interaction. The n is the adsorption intensity used for the trend prediction of adsorption. If n =1, the adsorption isotherm is a linear line; $n < 1$ refers to poor adsorptive potential, and $n > 1$ refers to the possibility of adsorption; titled (1/n) with a small value is related to the adsorbent-adsorbent bonding (Shikuku et al., 2021).

The adsorption isotherm is the relative adsorption capacity and concentration of residual adsorbent in solution at equilibrium. The Langmuir and Freundlich isotherms are shown in Figures 6(b) and 6(c). The parameters obtained from both isotherms are shown in Table 4. The adsorptions of methylene blue onto GBC, GSBC, FBC, FSBC, and SJBC were fitted with Langmuir isotherm with higher R^2. These results showed that this adsorption was monolayer adsorption on a homogeneous surface. Table 4 showed that the maximum adsorption of GSBC (200.0 mg/g) was higher than other adsorbents due to the high specific surface area (Table 1). However, a specific surface area was not the only factor affecting the adsorption; pore structures and functional groups were also involved (Wang et al., 2023). The adsorption capacity increases with the pore size of the adsorbent (Roslan et al., 2022). For the similar surface areas of FBC and FSBC, the latter showed greater values than those of FBC when a pore volume and average radius of porous were considered, as shown in Table 1. The effect of pore volume can also explain methylene blue adsorption capacity between FBC and SJBC. All these values affected the adsorption. The result was similar to the experiments of Goyal et al. (2004) for the insignificantly different surface areas and adsorption capacities. It was claimed that this may be due to the differences in the microporous and chemical properties of the carbon surface (Goyal et al., 2004). However, the maximum adsorption capacity of SJBC is 121.9 mg/g, which is lower than GSBC. This is because of the number of void volumes or pores caused by coagulation. The particles of SJBC aggregated tightly so that fewer pores were introduced. The minimum adsorption capacity for FBC was shown due to the small surface area and low porosity, which corresponded to Figure 1 and Table 1.

The adsorption capabilities of methylene blue onto different adsorbents are shown in Table 5. Non-activated carbon comparisons revealed that all samples fell within the competitive range. For further study, improving its quality could be able to adsorb similar to or better than other types of activated carbon.

Table 4. The determined parameters from Langmuir and Freundlich isotherms for the adsorption of methylene blue onto GBC, GSB, FBC, FSBC, and SJBC

Adsorbents	Parameters					
	Langmuir isotherm			Freundlich isotherm		
	b (L/min)	q_m (mg/g)	R^2	K_F (mg/g)(L/mg)$^{1/n}$	n	R^2
GBC	0.549	161.3	0.9858	76.23	4.836	0.9219
GSBC	7.143	200.0	0.9975	125.60	5.764	0.8491
FBC	0.112	75.8	0.9964	18.20	3.022	0.9458
FSBC	0.423	125.0	0.9876	55.12	4.525	0.9120
SJBC	0.323	121.9	0.9883	56.64	5.258	0.9783

Table 5. Adsorption capacities of methylene blue

Precursor	Activation reagent	Adsorption capacity (mg/g)	Sources
Rubber seeds	H_2SO_4	769.23	Nizam et al., 2021
Sucrose spherical carbon	KOH	704.2	Bedin et al., 2016
Un-sieved sugarcane bagasse	Water	148.8	El–Bery et al., 2022
Ackee apple pod	$ZnCl_2$	47.17	Bello et al., 2021
Deglat Beida stones	NaOH	163.67	Gherbia, et al., 2019
Chickpea stalk	$ZnCl_2$	105	Genli et al., 2021
Chickpea stalk hydrochar	None	45	Genli et al., 2021
Magnolia Grandiflora Linn leaf biochar	None	78.6	Ji et al., 2019
cosmetics industry, sewage sludge, Biochar	None	51.1	Ribeiro et al., 2021
Seaweed-based biochars	None	175	Güleç et al., 2022
Biochar from cocoa shell	None	163.5	Prabu et al., 2020
GBC	None	161.3	This study
GSBC	None	200.0	This study
FBC	None	75.8	This study
FSBC	None	125.0	This study
SJBC	None	122.0	This study

Thermodynamics study

The thermodynamics study used the methylene blue concentration of 40 mg/L at a pH of 7, contact time of 480 min, and temperatures of 25, 35, 45, and 50°C, respectively. Thermodynamic parameters, including enthalpy change (ΔH), entropy change (ΔS), and Gibbs free energy change (ΔG), are considerable for a better understanding of the effect of temperature on the adsorption process. This could be revealed if processes occur naturally (Estrada et al., 2021). For adsorption, it is already known that ΔH depends on electrostatic and Van der Waals interactions. Additionally, ΔS depends on hydrophobic interactions (Yoshida et al., 2020). The correlation of ΔG, ΔH, and ΔS is represented by equations (6), (7), and (8) (Liyanaarachchi et al., 2023; Tran, 2022).

$$\Delta G = \Delta H - T\Delta S \quad (6)$$

$$\ln K = -\frac{\Delta H}{RT} + \frac{\Delta S}{R} \quad (7)$$

$$K = \frac{q_e}{C_e} \quad (8)$$

The values of ΔH and ΔS can be obtained from the slope and intercept of the Van't Hoff plots as illustrated in Fig. 7. with ln K on the Y-axis versus $1/T$ on X-axis. R (8.314 J /mol K) is the gas constant, K is the equilibrium constant correlated with the Langmuir equation (Liu, 2009), and T (K) is the absolute temperature of the solution.

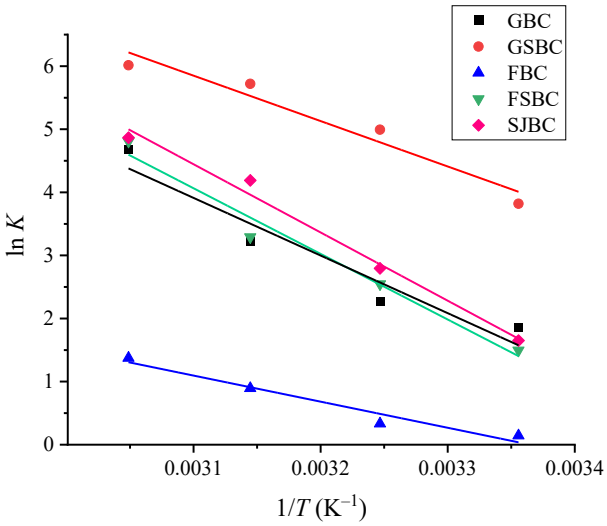

Figure 7. Van't Hoff plot of methylene blue removal by GBC, GSBC, FBC, FSBC, and SJBC.

From Table 6, the R^2 values of GBC, GSBC, FBC, FSBC, and SJBC were 0.9284, 0.9461, 0.9574, 0.9746 and 0.9881, respectively. The ΔH values of all samples were positive. This indicates that adsorption was an endothermic process. A positive value of ΔS represented a great affinity of MB^+ towards the adsorbent and increased randomness at the solid–solution interface (Tongpoothorn et al., 2020). ΔG was a negative value. It indicated that the adsorption capacity of MB^+ onto all samples could occur spontaneously. Basically, ΔH values of physisorption and chemisorption range from 2.1 to 20.9 kJ/mol and 80 to 200 kJ/mol, respectively (Amel et al., 2021).

The ΔH values of methylene blue adsorption for all samples represent the chemisorption process. This corresponded to the results of the pseudo-second-order model, which was similar to the experimental results of Liyanaarachchi et al. (2023). The ΔG values of physisorption and chemisorption range from 0 to –20.9 kJ/mol and –80 to –400 kJ/mol. However, it was reported that the activity coefficient affected the calculation of ΔG from the Langmuir equilibrium constant. This needs to be strictly considered due to the effect of the activity coefficient of a high-concentration solution (Liu, 2009). Tran (2022) reported that physisorption or chemisorption must depend on the magnitude of standard enthalpy change rather than standard Gibbs's free energy change.

Table 6. Thermodynamic parameters for the adsorption of methylene blue onto GBC, GSB, FBC, FSBC, and SJBC.

Adsorbents	ΔH (kJ/mol)	ΔS (J/mol K)	ΔG (kJ/mol)			
			25 °C	35 °C	45 °C	55 °C
GBC	75.95	267.96	–3.95	–6.63	–9.30	–11.98
GSBC	59.84	234.12	–9.97	–12.31	–14.65	–16.99
FBC	34.39	115.71	–0.11	–1.27	–2.43	–3.58
FSBC	86.47	301.87	–3.53	–6.55	–9.57	–12.59
SJBC	89.90	315.65	–4.21	–7.37	–10.52	–13.68

Effect of salt and existing ion

Salt and existing ions were investigated since most natural water, such as groundwater, canal water, seawater, and most wastewater, consists of several types of salt or ions. The type and concentration of salts or ions depend on the source and quality of the water. These may influence the adsorption of methylene blue. SJBC will be used to investigate the effects of salt and existing ions on methylene blue adsorption. This is because SJBC provided similar results of adsorption isotherm, kinetic, and thermodynamic effects. Besides, SJBC is produced for general purposes at a lower cost than GBS, GSBC, FBC, and FSBC, which are made from pure substances. The effect of salt was studied using a concentration of methylene blue of 40 mg/L under pH of 7, contact time of 480 min, and 25 ºC. The initial concentrations of NaCl and $MgCl_2$ were 5, 10, 15, and 20 g/L, respectively. It was found that increasing the concentration of NaCl and $MgCl_2$ decreased the adsorption capacity of methylene blue, as shown in Figure 8(a). The increasing salt concentration decreased the electrostatic attraction and electrostatic repulsion. The adsorption capacity is generally slightly increased when the ionic strength increases. As the experimental result, the adsorption capacity of methylene blue meanwhile decreased when the ionic strength increased. Consequently, the electrostatic attraction between methylene blue and SJBC was reduced and resulted in the adsorption capacity (Wang et al., 2022). From the experiment, it can be seen that Mg^{2+} had showed more effect on methylene blue adsorption than Na^{+} because of the effect of ionic strength. A decrease of active sites on the adsorbent and the active concentration of methylene blue occurred when the ionic strength increased. This is due to the interaction between positive and negative charges decreased. Therefore, at the same concentration of Mg^{2+} and Na^{+}, the effect of Mg^{2+} on adsorption capacity was greater than those of the latter, as theoretically expected. This might be because of the increased number of cations of Mg^{2+}, which can methylene blue cation adsorption (Guo et al., 2014).

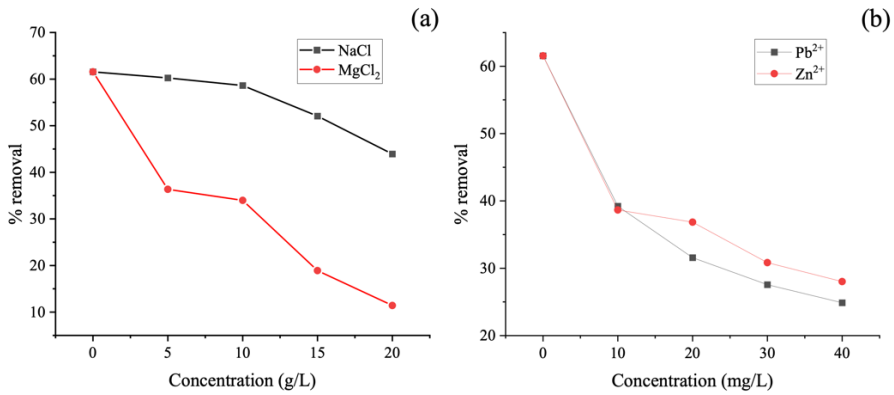

Figure 8. Effect of salt (a) and effect of coexisting ions (b) for methylene blue removal.

The coexisting ion was studied using 40 mg/L of methylene blue at pH 7, 25 ºC, and a contact time of 480 min. The initial concentrations of Pb^{2+} and Zn^{2+} were 10, 20, 30, and 40 mg/L, respectively. From Figure 8(b), the decrease in methylene blue adsorption of SJBC resulted from adsorption competition between the metal ions with methylene blue, as corresponded to the previous results of Ebadollahzadeh and Zabihi (2020) and Eltaweil et al. (2023). The existence of Pb^{2+} would affect the adsorption of methylene blue compared to Zn^{2+}. This is because Pb^{2+} can be better adsorbed. As previously reported, Pb^{2+} can be better absorbed on biochar than Zn^{2+} due to its lower binding energy (Zhao et al., 2020). The binding energies of Pb^{2+} and Zn^{2+} adsorbed on biochar were reported to be 139 and 1022 eV (Trakal et al., 2014; Gan et al., 2015). The binding energy of adsorption is related to the bond energy between the adsorbed molecule and the adsorbent (Yazaydin and Thompson, 2009).

Although SJBC suggested less adsorption capacity of methylene blue than GSBC and FSBC in this study, sugarcane juice is a cheaper precursor than pure glucose and fructose. SJBC can be substantially manufactured and used. Nonetheless, enhancing SJBC efficiency for further study could result in higher adsorption. The carbon from the rapid reaction of sugarcane juice with concentrated sulfuric acid can be used for the cation adsorption technique. Moreover, SJBC can also be applied to other adsorption applications such as antibiotics (Wang et al., 2020), methane (Shi et al., 2015), organic pollutants (Li et al., 2019), etc. or the use of other sugars in the synthesis of carbon (Tuli et al., 2020), such as sucrose (Choi and Park, 2015), white sugar (Xiao et al., 2020), molasses wastewater, etc.

CONCLUSIONS

SJBC was synthesized by rapid hydrolysis of sugarcane juice using concentrated sulfuric acid to produce adsorbent adsorption. It was found that the surface area of GBC and FBC was smooth and almost non-porous. On the other hand, synthesized GSBC, FSBC, and SJBC prepared from concentrated sulfuric acid and a solution suggested an aggregation of small particles, which affected the methylene blue adsorption. The adsorption kinetic study indicates that the adsorption of methylene blue onto all samples was performed under the pseudo-second-order model, which provided similar calculated and experimental q_e values. A study of the intra-particle diffusion model showed that the adsorption process occurred in two steps. The first step was rapid adsorption of methylene blue onto all the sample's surface. The second step was a slow diffusion within the adsorbent pore. The Langmuir model fits the methylene blue adsorption behavior onto all samples. This indicated a monolayer adsorption. GSBC, GBC, FSBC, SJBC, and FBC adsorption capacities were 200.0, 161.3, 125.0, 121.9, and 75.8 mg/g, respectively. The solution-produced GSBC and FSBC had more adsorption capacity of methylene blue than the powder-made GBC and FBC, respectively. The thermodynamic parameters represent the endothermic adsorption processes, the disorder and randomness at the solid-solution interface, and the spontaneity of adsorption. The values of ΔH and the pseudo-second-order model suggest that chemisorption is involved. Salts and metal ions that occurred during the process would negatively affect the methylene blue adsorption of SJBC. Using a solution such as sugarcane juice to convert into charcoal for adsorption by dehydration can remove methylene blue, which is the development of adsorbents from liquid natural products to remove other contaminants.

ACKNOWLEDGMENTS

The study was supported by Rajamangala University of Technology Lanna, Lampang. The authors sincerely thank the Department of Industrial Chemistry, Faculty of Science, Chiang Mai University, Chemistry Program, Faculty of Science, and Science and Technology Service Centre, Faculty of Science, Maejo University for analytical instruments support.

REFERENCES

Adekola, F. A., Ayodele, S. B., and Inyinbor, A. A. 2019. Activated biochar prepared from plantain peels: Characterization and Rhodamine B adsorption data set, Chemical Data Collections. 19: 100170. https://doi.org/10.1016/j.cdc.2018.11.012.

Alver, E., Metin, A. Ü., and Brouers, F. 2020, Methylene blue adsorption on magnetic alginate/rice husk bio–composite, International Journal of Biological Macromolecules. 154: 104–113. https://doi.org/10.1016/j.ijbiomac.2020.02.330.

Amador, C., and Martin de Juan, L. 2016. Chapter 19 – Strategies for structured particulate systems design. In: Computer Aided Chemical Engineering. Elsevier. p.509–579.

Amel, H., Yeddou–Mezenner, N., and Lounis, A. 2021. Eco–Friendly scolymus hispanicus for the Removal of Basic Blue 41, Iranian Journal of Chemistry and Chemical Engineering. 40(2): 511–523. https://doi.org/10.30492/ijcce.2020.38019.

Amran, F., and Zaini, M. A. A. 2021. Sodium hydroxide–activated Casuarina empty fruit: Isotherm, kinetics and thermodynamics of methylene blue and congo red adsorption, Environmental Technology & Innovation. 23: 101727. https://doi.org/10.1016/j.eti.2021.101727.

Arab, C., El Kurdi, R., and Patra, D., 2022. Zinc curcumin oxide nanoparticles for enhanced adsorption of congo red: kinetics and adsorption isotherms study, Materials Today Chemistry. 23: 100701. https://doi.org/10.1016/j.mtchem.2021.100701.

Aramesh, N., Bagheri, A. R., and Bilal, M. 2021. Chitosan-based hybrid materials for adsorptive removal of dyes and underlying interaction mechanisms, International Journal of Biological Macromolecules. 183: 399–422. https://doi.org/10.1016/j.ijbiomac.2021.04.158.

Badri, A., Alvarez–Serrano, I., Luisa López, M., and Ben Amara, M. 2020. Sol-gel synthesis, magnetic and methylene blue adsorption properties of lamellar iron monophosphate $KMgFe(PO_4)_2$. Inorganic Chemistry Communications. 121: 108217. https://doi.org/10.1016/j.inoche.2020.108217.

Bedin, K. C., Martins, A. C., Cazetta, A. L., Pezoti, O., and Almeida, V. C. 2016. KOH-activated carbon prepared from sucrose spherical carbon: Adsorption equilibrium, kinetic and thermodynamic studies for Methylene Blue removal. Chemical Engineering Journal. 286: 476–484. https://doi.org/10.1016/j.cej.2015.10.099.

Bello, M. O., Abdus–Salam, N., Adekola, F. A., and Pal, U. 2021. Isotherm and kinetic studies of adsorption of methylene blue using activated carbon from ackee apple pods. Chemical Data Collections. 31: 100607. https://doi.org/10.1016/j.cdc.2020.100607.

Bergna, D., Hu, T., Prokkola, H., Romar, H., and Lassi, U. 2020. Effect of some process parameters on the main properties of activated carbon produced from peat in a lab–scale process, Waste and biomass valorization. 11(6): 2837–2848. https://doi.org/10.1007/s12649–019–00584–2.

Chalmpes, N., Baikousi, M., Giousis, T., Rudolf, P., Salmas, C. E., Moschovas, D., Avgeropoulos, A., Bourlinos, A. B., Tantis, I., Bakandritsos, A., Gournis, D., and Karakassides, M. A. 2022. Biomass waste carbonization in piranha solution: A route to hypergolic carbons? Micro. 2(1): 137–153. https://doi.org/10.3390/micro2010009

Choi, Y. K., and Park, S. J. 2015. Preparation and characterization of sucrose–based microporous carbons for increasing hydrogen storage, Journal of Industrial and Engineering Chemistry. 28: 32–36. https://doi.org/10.1016/j.jiec.2015.02.012.

Corona, R. R. B., Sad, C. M. S., da Silva, M., Lopes, D. L., Leite, J. S. D., de F. Viegas, G. M., Gonçalves, G. R., Filgueiras, P. R., and de Castro, E. V. R. 2021. Adsorption of anionic surfactant in graphite oxide: A study for treatment of laundry wastewater, Journal of Environmental Chemical Engineering. 9(6): 106858. https://doi.org/10.1016/j.jece.2021.106858.

Dhar, L., Hossain, S., Rahman, M. S., Quraishi, S. B., Saha, K., Rahman, F., and Rahman, M. T. 2021. Adsorption mechanism of methylene blue by graphene oxide–shielded Mg-Al–layered double hydroxide from synthetic wastewater. The Journal of Physical Chemistry A. 125(4): 954–965. https://doi.org/10.1021/acs.jpca.0c09124.

Dolson, D. A., Battino, R., Letcher, T. M., Pegel, K. H., and Revaprasadu, N. 1995. Carbohydrate dehydration demonstrations. Journal of Chemical Education. 72(10): 927–929 https://doi.org/10.1021/ed072p927.

Ebadollahzadeh, H., and Zabihi, M. 2020. Competitive adsorption of methylene blue and Pb (II) ions on the nano–magnetic activated carbon and alumina. Materials Chemistry and Physics. 248: 122893. https://doi.org/10.1016/j.matchemphys.2020.122893.

El Maataoui, Y., Mrabet, M., Maaroufi, A., and Abdelmalek, D. 2019. Spiramycin adsorption behavior on activated bentonite, activated carbon and natural phosphate in aqueous solution. Environmental Science and Pollution Research. 26: 15953–15972. https://doi.org/10.1007/s11356–019–05021–4.

El–Bery, H. M., Saleh, M., El–Gendy, R. A., Saleh, M. R., and Thabet, S. M., 2022. High adsorption capacity of phenol and methylene blue using activated carbon derived from lignocellulosic agriculture wastes. Scientific Reports. 12(1): 5499. https://doi.org/10.1038/s41598–022–09475–4.

Eltaweil, A. S., Abd El–Monaem, E. M., El–Subruiti, G. M., Ali, B. M., Abd El-Latif, M. M., and Omer, A. M. 2023. Graphene oxide incorporated cellulose acetate beads for efficient removal of methylene blue dye; isotherms, kinetic, mechanism and co-existing ions studies. Journal of Porous Materials. 30(2): 607–618. https://doi.org/10.1007/s10934–022–01347–6.

Estrada, A. K. C, Lozano, F. C., and Díaz, R. A. L 2021. Thermodynamics and kinetic studies for the adsorption process of methyl orange by magnetic activated carbons. Air, Soil and Water Research. 14: 11786221211013336. https://doi.org/10.1177/11786221211013336.

Gan, C., Liu, Y., Tan, X., Wang, S., Zeng, G., Zheng, B., Li, T., Jiang, Z., and Liu, W. 2015. Effect of porous zinc–biochar nanocomposites on Cr(vi) adsorption from aqueous solution. RSC Advances. 5(44): 35107–35115. https://doi.org/10.1039/C5RA04416B.

Gautam, D., and Hooda, S. 2020. Magnetic graphene oxide/chitin nanocomposites for efficient adsorption of methylene blue and crystal violet from aqueous solutions. Journal of Chemical & Engineering Data. 65(8): 4052–4062. https://doi.org/10.1021/acs.jced.0c00350.

Genli, N., Şahin, Ö., Baytar, O., and Horoz, S. 2021. Synthesis of activated carbon in the presence of hydrochar from chickpea stalk and its characterization. Journal of Ovonic Research. 17(2): 117–124.

Geremias–Andrade, I. M., Rocheto, A. C., Gallo, F. A., and Petrus, R. R. 2020. The shelf life of standardized sugarcane juice stored under refrigeration. Food Science and Technology. 40(1): 95–101. https://doi.org/10.1590/fst.33918.

Gherbia, A., Chergui, A., Yeddou, A. R., Selatnia, A., and Nadjemi, B., 2019. Removal of methylene blue using activated carbon prepared from date stones activated with NaO. Global Nest Journal. 21(3): 374–380. https://doi.org/10.30955/gnj.002913.

Goyal, M., Singh, S., and Bansal, R. 2004. Equilibrium and Dynamic Adsorption of methylene blue from aqueous solutions by surface modified activated carbons. Carbon letters. 5.

Güleç, F., Williams, O., Kostas, E. T., Samson, A., Stevens, L. A., and Lester, E. 2022. A comprehensive comparative study on methylene blue removal from aqueous solution using biochars produced from rapeseed, whitewood, and seaweed via different thermal conversion technologies. Fuel. 330: 125428. https://doi.org/10.1016/j.fuel.2022.125428.

Guo, J. Z., Li, B., Liu, L., and Lv, K. 2014. Removal of methylene blue from aqueous solutions by chemically modified bamboo. Chemosphere. 111: 225–231. https://doi.org/10.1016/j.chemosphere.2014.03.118.

Ji, B., Wang, J., Song, H., and Chen, W. 2019, Removal of methylene blue from aqueous solutions using biochar derived from a fallen leaf by slow pyrolysis: Behavior and mechanism. Journal of Environmental Chemical Engineering. 7(3): 103036. https://doi.org/10.1016/j.jece.2019.103036.

Kalam, S., Abu–Khamsin, S. A., Kamal, M. S., and Patil, S. 2021. Surfactant adsorption isotherms: A Review, ACS Omega. 6(48): 32342–32348. https://doi.org/10.1021/acsomega.1c04661.

Khodmanee, S., and Amnuaylojaroen, T. 2021. Impact of biomass burning on ozone, carbon monoxide, and nitrogen dioxide in northern Thailand. 9: 641877. https://doi.org/10.3389/fenvs.2021.641877.

Khushboo, Kaur, M., and Jeet, K. 2022. Mechanistic insight into adsorption and photocatalytic potential of magnesium ferrite–bentonite nanocomposite. Journal of Photochemistry and Photobiology A: Chemistry. 425: 113717.https://doi.org/10.1016/j.jphotochem.2021.113717.

Kumar, R., Bhattacharya, S., and Sharma, P. 2021. Novel insights into adsorption of heavy metal ions using magnetic graphene composites. Journal of Environmental Chemical Engineering. 9(5): 106212. https://doi.org/10.1016/j.jece.2021.106212.

Li, K., Zhou, M., Liang, L., Jiang, L., and Wang, W. 2019. Ultrahigh–surface–area activated carbon aerogels derived from glucose for high–performance organic pollutants adsorption. Journal of Colloid and Interface Science. 546: 333–343. https://doi.org/10.1016/j.jcis.2019.03.076.

Liu, Y. 2009. Is the free energy change of adsorption correctly calculated?. Journal of Chemical & Engineering Data. 54(7): 1981–1985. https://doi.org/10.1021/je800661q.

Liyanaarachchi, H., Thambiliyagodage, C., Lokuge, H., and Vigneswaran, S. 2023. Kinetics and thermodynamics study of methylene blue adsorption to sucrose- and urea-derived nitrogen-enriched, hierarchically porous carbon activated by KOH and H_3PO_4. ACS Omega. 8: 16158–16173. https://doi.org/10.1021/acsomega.3c00339.

Lyu, R., Zhang, C., Xia, T., Chen, S., Wang, Z., Luo, X., Wang, L., Wang, Y., Yu, J., and Wang, C. 2020. Efficient adsorption of methylene blue by mesoporous silica prepared using sol-gel method employing hydroxyethyl cellulose as a template. Colloids and Surfaces A: Physicochemical and Engineering Aspects. 606: 125425. https://doi.org/10.1016/j.colsurfa.2020.125425.

Marrakchi, F., Hameed, B. H., and Bouaziz, M. 2020. Mesoporous and high-surface-area activated carbon from defatted olive cake by-products of olive mills for the adsorption kinetics and isotherm of methylene blue and acid blue 29. Journal of Environmental Chemical Engineering. 8(5): 104199. https://doi.org/10.1016/j.jece.2020.104199.

Mondal, S., and Majumder, S. K. 2019. Honeycomb–like porous activated carbon for efficient copper (II) adsorption synthesized from natural source: Kinetic study and equilibrium isotherm analysis. Journal of Environmental Chemical Engineering. 7(4): 103236. https://doi.org/10.1016/j.jece.2019.103236.

Naikwadi, P. M., Chavan, U. D., Pawar, V. D., and Amarowicz, R., 2010. Studies on dehydration of figs using different sugar syrup treatments. Journal of Food Science and Technology. 47(4): https://doi.org/442–445. 10.1007/s13197–010–0073–6.

Namal, O. O., and Kalipci, E. 2020. Adsorption kinetics of methylene blue removal from aqueous solutions using potassium hydroxide (KOH) modified apricot kernel shells. International Journal of Environmental Analytical Chemistry. 100(14): 1549–1565. https://doi.org/10.1080/03067319.2019.1656721.

Nizam, N. U. M., Hanafiah, M. M., Mahmoudi, E., Halim, A. A., and Mohammad, A. W. 2021. The removal of anionic and cationic dyes from an aqueous solution using biomass-based activated carbon. Scientific Reports. 11(1): 8623. https://doi.org/10.1038/s41598–021–88084–z.

Nkutha, C. S., Shooto, N. D., and Naidoo, E. B. 2020. Adsorption studies of methylene blue and lead ions from aqueous solution by using mesoporous coral limestones. South African Journal of Chemical Engineering. 34: 151–157. https://doi.org/10.1016/j.sajce.2020.08.003.

Noreen, S., Khalid, U., Ibrahim, S. M., Javed, T., Ghani, A., Naz, S., and Iqbal, M. 2020. ZnO, MgO and FeO adsorption efficiencies for direct sky Blue dye: equilibrium, kinetics and thermodynamics studies. Journal of Materials Research and Technology. 9(3): 5881–5893. https://doi.org/10.1016/j.jmrt.2020.03.115.

Oladoye, P. O., Ajiboye, T. O., Omotola, E. O., and Oyewola, O. J., 2022. Methylene blue dye: Toxicity and potential elimination technology from wastewater. Results in Engineering. 16: 100678. https://doi.org/10.1016/j.rineng.2022.100678.

Opoku, B. K., Isaac, A., Micheal, A. A., Bentum, J. K., and Muyoma, W. P. 2021. Characterization of chemically activated carbons produced from coconut and palm kernel shells using SEM and FTIR analyses. American Journal of Applied Chemistry. 9(3): 90–96.

Prabu, D., Kumar, P. S., Vardhan, K. H., Sathish, S., Raju, A., and Mathew, J. 2020, Adsorptive elimination of methylene blue dye from aquatic system using biochar produced from cocoa shell. Desalination and Water Treatment. 2020: 366–378. https://doi.org/10.5004/dwt.2020.26197.

Rehman, M. U., Manan, A., Uzair, M., Khan, A. S., Ullah, A., Ahmad, A. S., Wazir, A. H., Qazi, I., and Khan, M. A. 2021. Physicochemical characterization of Pakistani clay for adsorption of methylene blue: Kinetic, isotherm and thermodynamic study. Materials Chemistry and Physics. 269: 124722. https://doi.org/10.1016/j.matchemphys.2021.124722.

Rheima, A. M., Mahmood, R. S., Hussain, D. H., and Abbas, Z. S. 2021. Study the adsorption ability of alizarin red dye from their aqueous solution on synthesized carbon nanotubes. Digest Journal of Nanomaterials and Biostructures. 16(1): 11–18.

Ribeiro, M. R., de Moraes Guimarães, Y., Silva, I. F., Almeida, C. A., Silva, M. S. V., Nascimento, M. A., da Silva, U. P., Varejão, E. V., dos Santos Renato, N., Teixeira, A. P. d. C., and Lopes, R. P. 2021. Synthesis of value-added materials from the sewage sludge of cosmetics industry effluent treatment plant. Journal of Environmental Chemical Engineering. 9(4): 105367. https://doi.org/10.1016/j.jece.2021.105367.

Roslan, F. A. S., Harun, N. Y., Hezam, A. A., Saeed, R. M. R., Mannikam, S. D., and Al–Qadami, E. H. H., 2022. Methylene blue removal using palm oil mill effluent sludge–derived adsorbent. Chemical Engineering Transactions. 91: 589–594. https://doi.org/10.3303/CET2291099.

Sahoo, T. R., and Prelot, B. 2020. Chapter 7- Adsorption processes for the removal of contaminants from wastewater: the perspective role of nanomaterials and nanotechnology. In: Nanomaterials for the detection and removal of wastewater Pollutants. Elsevier. p.161–222.

Samoudi, B., Bendaou, O., Hanafi, I., Asselman, A., and Haboubi, K. 2022. FTIR and raman spectroscopy study of soot deposits produced in the infrared multiphoton dissociation of vinyl bromide. Journal of Spectroscopy. 2022: 9942870. https://doi.org/10.1155/2022/9942870.

Sattari, A., Ramazani, A., Aghahosseini, H., and Aroua, M. K. 2021. The application of polymer containing materials in CO_2 capturing via absorption and adsorption methods. Journal of CO_2 Utilization. 48: 101526. https://doi.org/10.1016/j.jcou.2021.101526.

Shi, J., Li, W. B., and Li, D. 2015. Rapidly reversible adsorption of methane with a high storage capacity on the zeolite templated carbons with glucose as carbon precursors. Colloids and Surfaces A: Physicochemical and Engineering Aspects. 485: 11–17. https://doi.org/10.1016/j.colsurfa.2015.08.026.

Shikuku, V. O., and Mishra, T. 2021, Adsorption isotherm modeling for methylene blue removal onto magnetic kaolinite clay: a comparison of two-parameter isotherms. Applied Water Science. 11(6): 103. 10.1007/s13201-021-01440-2.

Sparrevik, M., Adam, C., Martinsen, V., Jubaedah, and Cornelissen, G. 2015. Emissions of gases and particles from charcoal/biochar production in rural areas using medium-sized traditional and improved “retort” kilns. Biomass and Bioenergy. 72: 65–73. https://doi.org/10.1016/j.biombioe.2014.11.016.

Suhas, Gupta, V. K., Carrott, P. J. M., Singh, R., Chaudhary, M., and Kushwaha, S., 2016. Cellulose: A review as natural, modified and activated carbon adsorbent. Bioresource Technology. 216: 1066–1076. https://doi.org/10.1016/j.biortech.2016.05.106.

Sultana, M., Rownok, M. H., Sabrin, M., Rahaman, M. H., and Alam, S. M. N. 2022. A review on experimental chemically modified activated carbon to enhance dye and heavy metals adsorption. Cleaner Engineering and Technology. 6: 100382. https://doi.org/10.1016/j.clet.2021.100382.

Texixeira, G.G., and Santos, P. M. 2022. Simple and cost-effective approaches for quantification of reducing sugar exploiting digital image analysis. Journal of Food Composition and Analysis. 113 (2022): 104719. https://doi.org/10.1016/j.jfca.2022.104719.

Thang, N. H., Khang, D. S., Hai, T. D., Nga, D. T., and Tuan, P. D. 2021. Methylene blue adsorption mechanism of activated carbon synthesized from cashew nut shells. RSC Advances. 11(43): 26563–26570. https://doi.org/10.1039/D1RA04672A.

Tongpoothorn, W., Somboon, T., and Sriuttha, M. 2020. The utilization of Napier grass stems for Cd(II) Ions removal from aqueous solution: Process optimization studies using response surface methodology. Naresuan University Journal: Science and Technology. 28(3): 46–62. https://doi.org/10.14456/nujst.2020.25.

Trakal, L., Bingöl, D., Pohořelý, M., Hruška, M., and Komárek, M. 2014. Geochemical and spectroscopic investigations of Cd and Pb sorption mechanisms on contrasting biochars: Engineering implications. Bioresource Technology. 171: 442–451. https://doi.org/10.1016/j.biortech.2014.08.108.

Tran, H. N. 2022. Improper estimation of thermodynamic parameters in adsorption studies with distribution coefficient K_D (q_e/C_e) or Freundlich constant (K_F): Considerations from the derivation of dimensionless thermodynamic equilibrium constant and suggestions. Adsorption Science & Technology. 2022: 5553212. https://doi.org/10.1155/2022/5553212.

Tran, H. V., Hoang, L. T., and Huynh, C. D. 2020. An investigation on kinetic and thermodynamic parameters of methylene blue adsorption onto graphene-based nanocomposite. Chemical Physics. 535: 110793. https://doi.org/10.1016/j.chemphys.2020.110793.

Tuli, F. J., Hossain, A., Kibria, A. K. M. F., Tareq, A. R. M., Mamun, S. M. M. A., and Ullah, A. K. M. A. 2020. Removal of methylene blue from water by low–cost activated carbon prepared from tea waste: A study of adsorption isotherm and kinetics. Environmental Nanotechnology, Monitoring and Management. 14: 100354. https://doi.org/10.1016/j.enmm.2020.100354.

Wang, B., Lan, J., Bo, C., Gong, B., and Ou, J. 2023. Adsorption of heavy metal onto biomass-derived activated carbon: review. Royal Society of Chemistry. 13: 4275-4302. https://doi.org/10.1039/D2RA07911A.

Wang, B., Xu, X., Tang, H., Mao, Y., Chen, H., and Ji, F. 2020. Highly efficient adsorption of three antibiotics from aqueous solutions using glucose-based mesoporous carbon. Applied Surface Science. 528: 147048. https://doi.org/10.1016/j.apsusc.2020.147048.

Wang, J., Ma, J., and Sun, Y. 2022. Adsorption of methylene blue by coal-based activated carbon in high–salt wastewater. Water. 14(21): 3576.

Wang, N. S. 2004. Experimental No.9D Sucrose assay by the dinitrosalicylic colorimetric method. https://user.eng.umd.edu/~nsw/ench485/lab9d.htm

Wang, S. N., Li, P., Gu, J. J., Liang, H., and Wu, J. H. 2018. Carboxylate–functionalized sugarcane bagasse as an effective and renewable adsorbent to remove methylene blue. Water Science and Technology. 2017(1): 300–309. https://doi.org/10.2166/wst.2018.113.

Whitener, J. K. E. 2016. Rapid synthesis of thin amorphous carbon films by sugar dehydration and dispersion. AIMS Materials Science. 3(4): 1309–1320. https://doi.org/10.3934/matersci.2016.4.1309.

Wibawa, P. J., Nur, M., Asy'ari, M., and Nur, H. 2020. SEM, XRD, and FTIR analyses of both ultrasonic and heat-generated activated carbon black microstructures. Heliyon. 6(3): e03546. https://doi.org/10.1016/j.heliyon.2020.e03546.

Wu, K. H., Huang, W. C., Hung, W. C., and Tsai, C. W. 2021. Modified expanded graphite/Fe_3O_4 composite as an adsorbent of methylene blue: Adsorption kinetics and isotherms. Materials Science and Engineering: B. 266: 115068. https://doi.org/10.1016/j.mseb.2021.115068.

Wu, Q., Dong, S., Wang, L., and Li, X. 2021. Single and competitive adsorption behaviors of Cu^{2+}, Pb^{2+} and Zn^{2+} on the biochar and magnetic biochar of Pomelo peel in aqueous solution. Water. 13(6): 868.

Xiao, W., Garba, Z. N., Sun, S., Lawan, I., Wang, L., Lin, M., and Yuan, Z. 2020. Preparation and evaluation of an effective activated carbon from white sugar for the adsorption of rhodamine B dye. Journal of Cleaner Production. 253: 119989. https://doi.org/10.1016/j.jclepro.2020.119989.

Yazaydin, A. O., and Thompson, R. W. J. E. E. S. 2009. Computing adsorbate/adsorbent binding energies and Henry's law constants from molecular simulations. Environmental Engineering Science. 26: 297–303. https://doi.org/10.1089/EES.2008.0025

Yoshida, Y., Shimada, T., Ishida, T., and Takagi, S. 2020. Thermodynamic study of the adsorption of acridinium derivatives on the clay surface. RSC Advances. 10: 21360–21368. https://doi.org/10.1039/D0RA03158E.

Zaidan, N. L., Mohamad–Fuzi, S. F., Hailan, I. M., Roshidi, A. A., Kormin, F., Abu–Bakar, M. F., and Sabran, S. F. 2021. Physicochemical and sensory characteristics of treated sugarcane juice, In: IOP Conference Series: Earth and Environmental Science, International Conference on Biodiversity. Melaka, 4-5 November 2020. IOP Publishing, Philadelphia. p.012073.

Zhang, Y., Xu, J., Li, B., Xie, Z., Li, X., Tang, J., and Fan, S. 2021, Enhanced adsorption performance of tetracycline in aqueous solutions by KOH-modified peanut shell-derived biochar. Biomass Conversion and Biorefinery. https://doi.org/10.1007/s13399-021-02083-8.

Zhao, M., Dai, Y., Zhang, M., Feng, C., Qin, B., Zhang, W., Zhao, N., Li, Y., Ni, Z., Xu, Z., Tsang, D. C. W., and Qiu, R. 2020. Mechanisms of Pb and/or Zn adsorption by different biochars: Biochar characteristics, stability, and binding energies. Science of the Total Environment. 717: 136894. https://doi.org/10.1016/j.scitotenv.2020.136894.

Zhou, Q., Liao, B., Lin, L., Qiu, W., and Song, Z. 2018. Adsorption of Cu(II) and Cd(II) from aqueous solutions by ferromanganese binary oxide-biochar composites. Science of the Total Environment. 615: 115–122. https://doi.org/10.1016/j.scitotenv.2017.09.220.